New proton conducting nanocomposite membranes based on poly vinyl alcohol/poly vinyl pyrrolidone/BaZrO₃ for proton exchange membrane fuel cells

Abdol Mohammad Attaran [a], Mehran Javanbakht [b,c,*], Khadijeh Hooshyari [b,c], Morteza Enhessari [c,d]

[a] Department of Chemistry, Payame Noor University (PNU), Tehran, Iran
[b] Department of Chemistry, Amirkabir University of Technology, Tehran, Iran
[c] Fuel Cell and Solar Energy Lab, Renewable Energy Research Center, Amirkabir University of Technology, Tehran, Iran
[d] Department of Chemistry, Naragh Branch, Islamic Azad University, Naragh, Iran

ARTICLE INFO

ABSTRACT

In this study for the first time, BaZrO₃ nanoparticles as mixed metal oxides, with provision of strong acid sites and good hydrophilic nature were used for the preparation of organic–inorganic proton exchange membranes. Poly(vinyl alcohol)–BaZrO₃ (PB) and poly(vinyl alcohol)/poly(vinyl pyrrolidone)–BaZrO₃ (PPB) nanocomposite membranes have been prepared. PPB nanocomposite membranes containing 1 wt.% of BaZrO₃ nanoparticles demonstrated high proton conductivity (6.01×10^{-2} S/cm) at 70 °C. The highest peak power density of 28.98 mW/cm² at $E_{p,max}$ of 0.14 V with a peak current density ($i_{p,max}$) of 201 mA/cm² was achieved for the PEMFC which included PPB nanocomposite membranes at 70 °C.

© 2014 Elsevier B.V. All rights reserved.

1. Introduction

Proton exchange membrane fuel cells (PEMFCs) are generally accepted as attractive conventional power sources, due to their high efficiency and lack of pollution [1,2]. Perfluorosulfonated ionomers, such as Nafion, are one of the most advanced commercially available membranes for PEMFCs because of their excellent chemical and thermal stability, good mechanical strength and high proton conductivity [3]. However, Nafion membrane applications in PEMFCs are still limited by operation at temperatures below 80 °C, high cost and methanol crossover [4]. Therefore, preparation of composite membranes with low cost and high proton conductivity to replace commercial Nafion membrane has been the challenge of continuous researches. Poly(vinyl alcohol), PVA, is highly hydrophilic, nontoxic and low cost polymer with excellent film forming property. PVA films have good chemical and mechanical stabilities and high potential for chemical crosslinking [5,6]. These properties of PVA must be considered by researchers, but low proton conductivity and high swelling (even dissoluble in water at higher temperature) of PVA membrane limit its application in PEMFCs [7]. According to a new research report, addition of hygroscopic metal oxide nanoparticles such as titanium oxide, zirconium oxide and zeolite in a PVA matrix improves its water uptake and proton conductivity [8]. One of the effective approaches is to blend PVA with hydrophilic polymers such as Nafion, sPEEK and poly(styrene sulfonic acid-co-maleic acid) (PSSA-MA). Hydrophilic polymers increase the proton conductivity of PVA based membrane [9]. Several researches have used an aldehyde and dialdehyde to crosslink of PVA and control its mechanical stability [10]. Previous researches have used sulfonation agents, such as sulfoacetic acid, and sulfosuccinic acid (SSA) as crosslinking agents to prepare PVA based membranes [11].

In previous studies, we introduced new proton conducting hybrid membranes for PEM fuel cells based on poly(vinyl alcohol) and nanoporous silica containing phenyl or propyl sulfonic acid [12,13] and poly(vinyl alcohol) and poly(sulfonic acid)-grafted silica nanoparticles [14,15]. Recently, the preparation and characterization of Nafion/Fe₂TiO₅ nanocomposite membranes for proton exchange membrane fuel cells (PEMFCs) were investigated [16]. The prepared Fe₂TiO₅ nanocomposite membranes showed a higher water uptake, proton conductivity and thermal stability compared with the pure commercial Nafion membranes. The highest proton conductivity (226 mS/cm) was observed for the membranes containing 2 wt.% of Fe₂TiO₅ nanoparticles and prepared in de-ionized water (DI) as solvent.

Protonic conductors with perovskite structure have been particularly studied due to their high chemical stability, excellent thermal and

* Corresponding author at: Department of Chemistry, Amirkabir University of Technology, Tehran, Iran. Tel.: +98 21 64542764; fax: +98 21 64542762.
E-mail address: mehranjavanbakht@gmail.com (M. Javanbakht).

mechanical stabilities, relatively low cost and high applicability in electrochemical devices for energy generation. Therefore, the investigation and knowledge of their proton transport properties are of countless concentration and significant to extend the potentials of application in industrial scale method [17].

$BaZrO_3$ with considerable levels of protonic conductivity has a great potential for use in fuel cells [16,18,19]. $BaZrO_3$ a proton conductor with a simple cubic perovskite structure has much attention for its applications in a PEMFC such as: poor thermal conductivity, excellent mechanical and structural integrities under extreme thermal excursions [20] and high chemical stability. The name perovskite currently is commonly employed to name a specific group of oxides with a common formula of ABO_3. A perovskite-type oxide typically expressed by ABO_3 is structurally stable because of its well-balanced geometrical array of constituent atoms and their valences [16]. Compared to other oxide families such as pyrochlore, perovskite related compounds can be synthesized with extensive variation of arrangements of chemical elements, because cations of large (site A) and small (site B) ionic radius fit well in the crystalline structure and in addition that structure is extremely tolerant to vacancy formation. In these oxides with formula ABO_3, the A-site can be occupied by cations M^+ (Na, K), M^{2+} (Ca, Sr, Ba) or M^{3+} (Fe, La, Gd) and B-site can be occupied either by M^{5+} (Nb, W), M^{4+} (Ce, Zr, Ti) or M^{3+} (Mn, Fe, Co, Ga) [17].

Between the perovskites with cubic structures, $BaZrO_3$ is a refractory ceramic material which is exactly promising due to its high melting point (2920 °C) and low chemical reactivity with corrosive compounds; it is the solitary ceramic material that does not follow phase transitions over the range from 1327 °C down to 269 °C [21, 22].

In the present work, poly (vinyl alcohol)/poly(vinyl pyrrolidone)–$BaZrO_3$ nanocomposite membranes were prepared by solution casting method. The –OH groups of $BaZrO_3$ nanoparticles, as mixed metal oxides, provide strong hydrogen bonding sites and increase the contents of the bound to free water ratio into the membrane matrix. The structure, water uptake, proton conductivity, morphology, thermal stability and mechanical properties of nanocomposite membranes were investigated. The $BaZrO_3$ nanoparticle content and poly(vinyl pyrrolidone) (PVP) effects on the water uptake and proton conductivity, as two important parameters, were evaluated in this study.

2. Experimental

2.1. Materials

Poly(vinyl alcohol), PVA, 99 +% hydrolyzed, with an average molecular weight of 145,000 was used as supplied by Merck. The cross-linking agent was a 25 wt.% solution of glutaraldehyde (GA) in water (Merck). Poly(vinyl pyrrolidone) (average MW = 40,000) was purchased from Sigma-Aldrich and used as blend polymer with PVA membrane. All solvents were purchased from Sigma-Aldrich. $BaZrO_3$ nanoparticles with a particle size range of 20 to 25 nm were used as modifier.

2.2. Synthesis of $BaZrO_3$ nanoparticles

$BaZrO_3$ nanoparticles were prepared according to the literature procedure [23]: An appropriate amount of stearic acid was first melted in a beaker at 73 °C. Subsequently, barium stearate was added. After that, stoichiometric tetrabutyl zirconate was added to the resulted green transparent solution and stirred to form a homogeneous light sol. Then the sol was naturally cooled down to room temperature, and dried in an oven for 12 h to obtain dried gel. The prepared gel was calcined in air to obtain nano-crystallites of $BaZrO_3$.

2.3. Preparation of membranes

The PVA based membranes were obtained by dissolving appropriate amounts of PVA and $BaZrO_3$ nanoparticle, in de-ionized (DI) water

under stirring at 80 °C. Water solutions of PVP were separately prepared and mixed with PVA solution (PVA:PVP 76:23). Then GA was gradually added. The resulting solution was stirred at 80 °C until becoming homogeneous and viscous. The well-mixed solution was cast into petri-glass dishes and allowed to dry and solidify for 24 h at room temperature. When visually dried, the membrane was dislodged from the petri-glass dishes easily. The prepared nanocomposite membranes were then stored in DI water to be kept hydrated for other process. PVA–$BaZrO_3$ and PVA–PVP–$BaZrO_3$ nanocomposite membranes were named PB and PPB, respectively. PB_x and PPB_x samples were named for x wt.% of the nanoparticles.

2.4. Water uptake and oxidative durability of membranes

The swelling of the membranes was evaluated in terms of their water uptake. Water uptake was determined as reported before [12]. The membrane was equilibrated in de-ionized water at room temperature for 24 h. The wet membrane was removed and the remaining water on the surface was dried by tissue papers, finally weighted instantly. For dried weight, the membrane was dried in oven at 80 °C for 24 h, and then weighted immediately. This process was reiterated for several times until reaching a stable result. The water uptake was calculated from Eq. (1).

$$Water\ uptake\% = \frac{W_{wet} - W_{dry}}{W_{dry}} \times 100 \tag{1}$$

where, W_{wet} and W_{dry} are weights of wet and dry membranes, respectively.

Oxidative stabilities were determined using Fenton's reagent (30 ppm $FeSO_4$ in 30% H_2O_2) at 50 °C and 70 °C. A small piece of membranes was immersed in Erlenmeyer flask containing Fenton's reagent. The stability was estimated by recording the time when membranes began to break.

2.5. Water uptake measurements of nanoparticles

The water uptake of the nanoparticles was calculated by the following Eq. (2).

$$WU_{NP} = \frac{W_{w,NP} - W_{d,NP}}{W_{d,NP}} \times 100 \tag{2}$$

where, $W_{w,NP}$ and $W_{d,NP}$ are weights of the wet and dry nanoparticles, respectively. To determine the wet weight of the nanoparticles, a certain amount of nanoparticles was put into a test tube in 100% RH for 24 h. The fully hydrated nanoparticles were then removed from the test tube and weighted instantly. To obtain the dry weight of the nanoparticles, they were placed in an oven at 80 °C for 24 h, and then weighted immediately. The same procedure was repeated several times to ensure that the results are real.

2.6. Proton conductivity measurements

The proton conductivity of membranes was calculated by the AC impedance spectroscopy with PGSTAT303N potentiostat/galvanostat (Ecochemie). The sample membrane was immerged in de-ionized water for 24 h at room temperature and then sealed between two platinum plate electrodes. The measurements were carried out on the potentiostatic mode. The spectra were recorded with signal amplitude of 50 mV in the frequency range of 100 Hz–1 MHz with 100 points. The resistance of the membrane was obtained from the high-frequency intercept of the impedance. The conductivity values were calculated by using the equation (σ = L/RS), where, σ, L, R, and S respectively refer to, proton conductivity (S/cm), thickness (cm), resistance from the impedance data (Ω) and cross-sectional area (cm^2) of the membranes.

2.7. FT-IR ATR spectra

The FT-IR ATR spectra (600–4000 cm^{-1}, resolution of 4 cm^{-1}) were recorded with a Bruker Equinox 55 using an attenuated total reflectance (ATR, single reflection) accessory purged with ultra dry compressed air.

2.8. SEM and EDX measurements

The morphology of nanocomposite membranes was investigated by using a scanning electron microscopy (SEM), (JSM-5600, Jeol Co.), coupled with energy dispersive X-ray (EDX) spectroscopy. The samples were freeze-fractured in liquid N$_2$ and coated with gold plate before SEM observations were carried out.

2.9. Thermal and mechanical properties

Thermogravimetric analysis (TGA) of the nanocomposite membranes was carried out by using a TGA/TA Instruments 2050 system, at a heating rate of 20 °C/min in nitrogen atmosphere from 25 to 600 °C. For determining mechanical properties at first membranes were dried and then mechanical properties of the prepared membranes were measured by using Zwick/Roell Z030 tensile test machine. All the membranes were cut to the standard shape and all tests were performed at a crosshead speed of 10 mm/min and room temperature (25 °C).

2.10. MEA and fuel cell tests

2.10.1. Preparation of microporous layer on the carbon paper

In order to prepare carbon ink for the microporous layer (MPL) of gas diffusion layer (GDL), slurry of carbon powder (acetylene black) (70–30 wt.%) with PTFE (60 wt.% PTFE) dispersion in a mixture of isopropyl alcohol/de-ionized water mixture (90–10 volume ratio) and glycerol (0.8 ml) was prepared by ultrasonication followed by magnetic stirring. The resulting carbon ink was painted onto one side of the carbon papers pretreated with 10 wt.% PTFE (SGL 10CA, SGL Carbon Group), followed by drying at 80 °C for 30 min. The GDL samples were heat-treated at 280 °C for 30 min to evaporate all remaining glycerol, and then at 350 °C for 30 min to uniformly distribute PTFE throughout the MPL. In the MPL, the carbon loading was 1 mg cm^{-2}.

2.10.2. Preparation of MEA

The catalyst slurry ink of the anode and cathode was prepared by using Pt-C (20%), 15 wt.% Nafion binder solution (Aldrich), and a suitable amount of distilled water and isopropyl alcohol (IPA). The resulting Pt-C inks were first ultrasonicated for 1 h to break up the catalyst
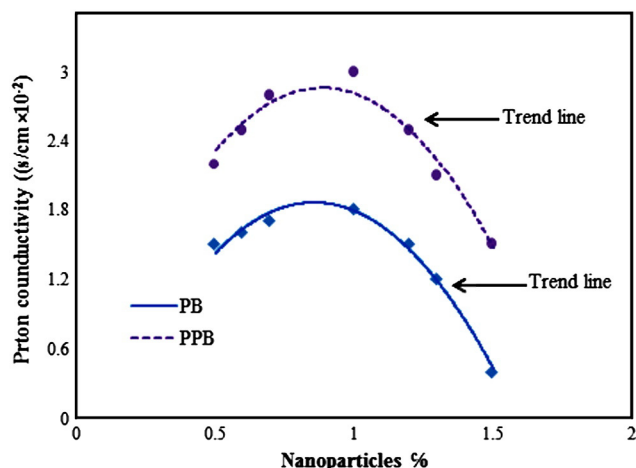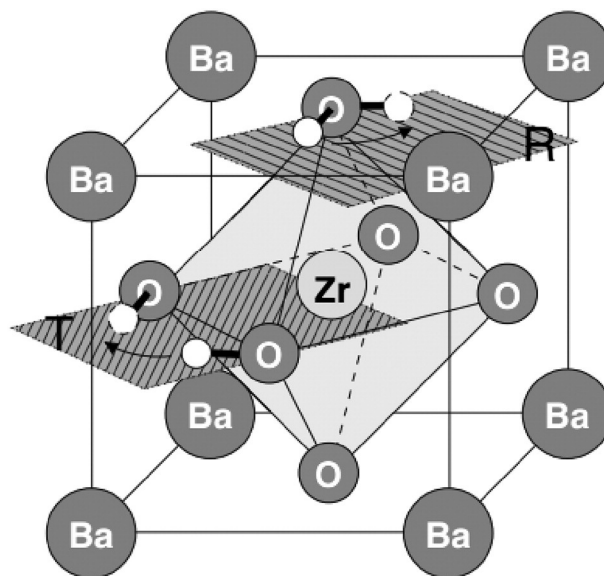

Fig. 2. Schematic illustration of the proton transfer (T) and reorientation (R) pathways in the cubic perovskite structure of BaZrO$_3$. The small white balls represent the energy minimum position of the proton [25].

powder and obtain a homogenous ink. The Pt-C inks were loaded onto the carbon paper (containing MPL) by a painting method to achieve a loading of 0.5 mg cm^{-2}. The as-prepared electrodes were dried in a vacuum oven at 80 °C for 30 min and 120 °C for 1 h. The Pt loading on each electrode was measured by the difference in weight before and after painting. Membrane electrode assembly (MEA) with an active area of 5 cm^2 was obtained by hot pressing the cathode and anode sandwiched with the PPB$_1$ nanocomposite membrane at 25 °C under 100 kgf cm^{-2} for 15 min. The flow rates for both hydrogen and oxygen gases were kept as 200 ml/min and 500 ml/min respectively. Polarization curves were obtained using a fuel cell evaluation system (FCT-150 s) in the 25 °C, 50 °C and 70 °C.

3. Results and discussion

3.1. Water uptake and proton conductivity measurements

The nanocomposite membrane based PVAs were prepared with 0.5–1.5 wt.% (0.5, 0.6, 0.7, 1, 1.2, 1.3 and 1.5 wt.%) of BaZrO$_3$ nanoparticles. PB and PPB nanocomposite membranes displayed higher proton conductivity than that of PVA (5.01 × 10^{-4} S/cm) based membranes (Fig. 1). This improvement was attributed to the hydrophilic nature of BaZrO$_3$ nanoparticles and PVP [24] within the PVA matrix.

Proton conduction in BaZrO$_3$ nanoparticles, results from their ability to dissolve protons from water in wet atmospheres [16]. Protons are incorporated into BaZrO$_3$ nanoparticles by dissociative adsorption of water molecules at the surface, followed by diffusion toward the nanoparticles' interior [17]. Schematic design of the proton transfer (T) and reorientation (R) pathways in the cubic perovskite structure of BaZrO$_3$ are displayed in Fig. 2 [25]. In the Grotthus mechanism for proton transport (T) in BaZrO$_3$ nanoparticles, proton diffuses by an arrangement between a molecular reorientation (R) round the oxygen and jump of

Fig. 1. Proton conductivity of PB and PPB nanocomposite membranes at 25 °C.

Table 1
Specification of synthesized PVA nanocomposite membranes at 25 °C.

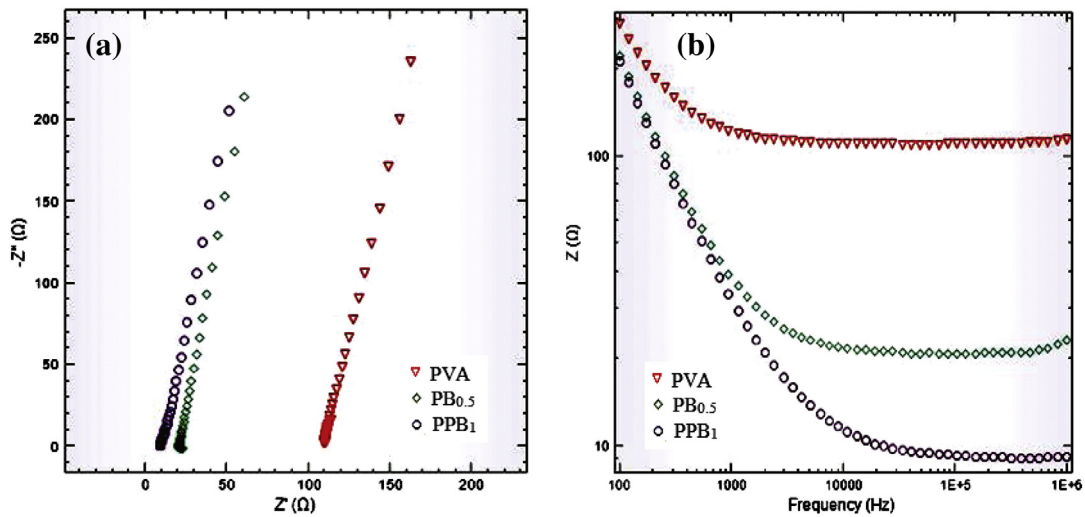| Membranes	Water uptake %	Proton conductivity (S/cm × 10^{-2})	Elongation at break (%)	Tensile strength (MPa)
PPB$_1$	220	3	21.55	100.5
PB$_1$	195	1.8	6.27	30.53
PVA	180	0.05	5.23	25.29

Fig. 3. Nyquist (a) and Bode Modulus (b) plots of PVA, PB$_1$ and PPB$_1$ membranes under fully hydrated condition at 25 °C.

the proton from oxygen to a nearest neighbor ion [17,25,26]. The orientation of the O–H group directs H$^+$ near to the neighboring oxygen ion. The rotation period (10–12 s) and jumping time (~9–10 s) are low in which is considered the limiting step of the conduction mechanism [27–30]. The strong interaction between the proton and the two oxygen neighbors avoids the need of extra energy to break the O–H bond [31]. Thus, a non-stoichiometric perovskite such as oxygen-deficient ABO$_{3-\delta}$, A-deficient A$_{1-\delta}$BO$_3$, or B-deficient AB$_{1-\delta}$O$_3$ often appears, where δ expresses the number of deficient atoms per unit formula. In the first case, an oxygen vacancy would be formed [16]. Hydroxide group from water dissociation fills the vacant oxygen site, whereas proton forms chemical bonding with lattice oxygen [28].

PPB nanocomposite membranes demonstrated higher proton conductivity than PB nanocomposite membranes. PVP owing to high polarity of –N–C=O group has good hydrophilic nature and made strong hydrogen-bonding with water which result in an increase in the water uptake and proton conductivity of PPB nanocomposite membranes. PB$_1$ demonstrated the highest proton conductivity (1.8×10^{-2} S/cm) compared with other PB nanocomposite membranes at 25 °C. PPB$_1$ nanocomposite membranes displayed higher water uptake (220%) and proton conductivity (3.01×10^{-2} S/cm) than PVA, PB and other PPB membranes at 25 °C. Table 1 and Fig. 1 confirm these results. Similar results for water uptake have been observed in previous work [12,13,32]. The results obtained from water uptake measurements of BaZrO$_3$

nanoparticles demonstrated that those BaZrO3 nanoparticles displayed a 9% water uptake in 25 °C. This result confirms that the BaZrO$_3$ nanoparticles have hydrophilic nature.

The Nyquist and Bode Modulus plots for PVA, PB$_1$ and PPB$_1$ membranes were shown in Fig. 3, under fully hydrated condition at 25 °C. PPB$_1$ nanocomposite membranes displayed a lower resistance (higher proton conductivity) than that of the PB$_1$ and PVA membranes, this result has been displayed in Fig. 3(a). Bode Modulus plots (Fig. 3(b)) showed lower resistance for PPB$_1$ nanocomposite membrane corresponds to the Nyquist plots. Bode Modulus plots also show that the lowest resistance is observed at the highest frequency [33,34]. Hence according to the equation ($\sigma = L/RS$), a resistance at low frequencies in the Nyquist plot was used to achieve the proton conductivity.

Fig. 4 represents the temperature dependence of proton conductivity for PPB$_1$ and PB$_1$ nanocomposite membranes. It has been found that the proton conductivity of the PPB$_1$ and PB$_1$ nanocomposite membranes increases with increasing temperature (Table 2).

The proton conductivity value of PPB$_1$ and PB$_1$ nanocomposite membranes was 6.01×10^{-2} and 3.9×10^{-2} S/cm at 70 °C, respectively.

The change in conductivity with temperature in solid polymer electrolyte can be attributed to segmental (i.e., polymer chain) motion, which results in an increase in the free volume of the system. Thus, the segmental motion either permits the ions to hop from one site to another or provides a pathway for ions to move. In other words, the segmental movement of the polymer facilitates the translational ionic motion [35].

Table 3 displays a comparison between the proton conductivity of new nanocomposite membranes and the other works in different temperatures [35–44]. As can be seen, the PPB$_1$ nanocomposite membranes demonstrated significant proton conductivity (6.01×10^{-2} S/cm at 70 °C) in comparison to PVA nanocomposite membranes [40,42,43]. This improvement in the proton conductivity of PPB$_1$ nanocomposite membranes was attributed to the excellent proton transfer mechanism in the BaZrO$_3$ nanoparticles structure which increases proton transfer pathways. Another reason for high proton conductivity of PPB$_1$ nanocomposite membranes was strong hydrogen-bonding of PVP with water. The results showed that, the water uptake of the synthesized nanocomposite
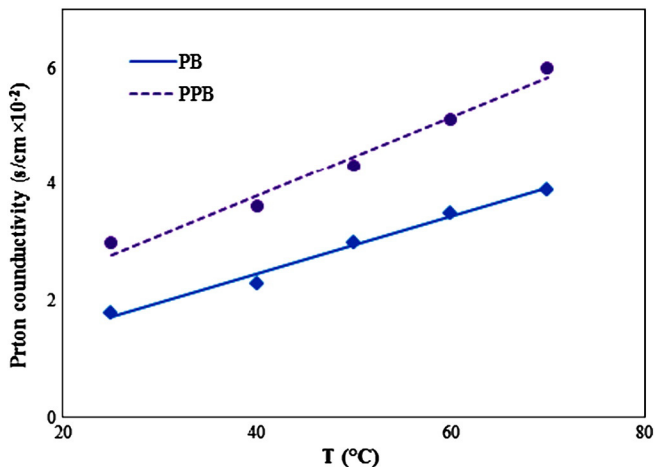

Fig. 4. Proton conductivity of PPB$_1$ and PB$_1$ nanocomposite membranes in the different temperatures.

Table 2
Proton conductivities for PVA nanocomposite membranes at various temperatures.

Membrane	$\sigma/(S/cm \times 10^{-2})$				
	25 °C	40 °C	50 °C	60 °C	70 °C
PPB$_1$	3.02	3.61	4.31	5.11	6.01
PB$_1$	1.8	2.3	3.01	3.5	3.9

Table 3
Comparison of proton conductivity of several PVA membranes in different temperatures.

Membrane	Temperature (°C)	Proton conductivity (S/cm $\times 10^{-2}$)	Ref
PPB$_1$	25	3	This work
	70	6	This work
Nafion 117	25	1.34	9
	80	6.2	36
PVA based membranes	25	0.62	37
	25	4.6	38
	25	2	39
	25	0.1	40
	60	6.23	7
	65	1.7	35
	70	5.95	32
	75	4	41
	80	0.48	42
	90	2.6	43
	100	0.8	44

membranes was higher than commercial Nafion 117 membrane and their proton conductivity was successfully comparable to that.

According to the high surface energy of BaZrO$_3$ nanoparticles, they have chemical interactions with the environment; therefore they are extremely unstable. Hence, their self-aggregation leads to a decrease in their specific surface and consequently in their water uptake and proton conductivity. So BaZrO$_3$ nanoparticle content, as a key parameter in the manufacturing of nanocomposite membranes, was investigated in this study. Fig. 1 shows that addition of high BaZrO$_3$ nanoparticles content (>1 wt.%) decreases the proton conductivity of PB and PPB nanocomposite membranes. These results can be attributed to the self-aggregation of the nanoparticles inside the membranes. Fig. 5 shows the SEM images of the cross-section of PPB nanocomposite membranes with different contents of BaZrO$_3$ nanoparticles. Fig. 5(a) indicates that the PPB$_1$ nanocomposite membrane is homogenous. The PPB$_{1.2}$ nanocomposite membranes are no longer homogenous (Fig. 5(b). Significant agglomerations of BaZrO$_3$ nanoparticles were clearly visible in the PPB$_{1.5}$ nanocomposite membranes (Fig. 5(c)). These images show that the aggregation of BaZrO$_3$ nanoparticles is occurred at high content of nanoparticles. The agglomeration of nanoparticles leads to a decrease in the active surface area of the nanoparticles and accordingly the membrane water uptake is decreased. Hence, large quantities of nanoparticles in the cross-section of PPB$_{1.5}$ nanocomposite membranes, lead to the accumulation of nanoparticles in these samples.

3.2. Oxidative durability

To evaluate the oxidative durability of PPB$_1$ nanocomposite membranes, time dependent measurements of the weight changes in Fenton's reagent at 50 °C and 70 °C were carried out. As can be seen in Fig. 6, a primary sharp decrease in weight percentage was observed after the PPB$_1$ nanocomposite membranes were soaked in Fenton's reagent within 30 h. After that, the weight of nanocomposite membranes tends to maintain a constant value with no further weight losses again up to 150 h. PPB$_1$ nanocomposite membranes because of their high cross-linked structure at 70 °C compared with 50 °C, which may make the PVA chain to be less attacked by water molecules containing oxidizing radical species, exhibited a good oxidative stability at 70 °C. The result shows that the PVA nanocomposite membranes attain promising oxidation stability for application in PEMFCs.

3.3. FT-IR ATR spectra

Fig. 7 shows a typical ATR spectra measured for PVA and PPB$_1$ membranes. The broad bands at around 3200–3600 cm^{-1} are observed
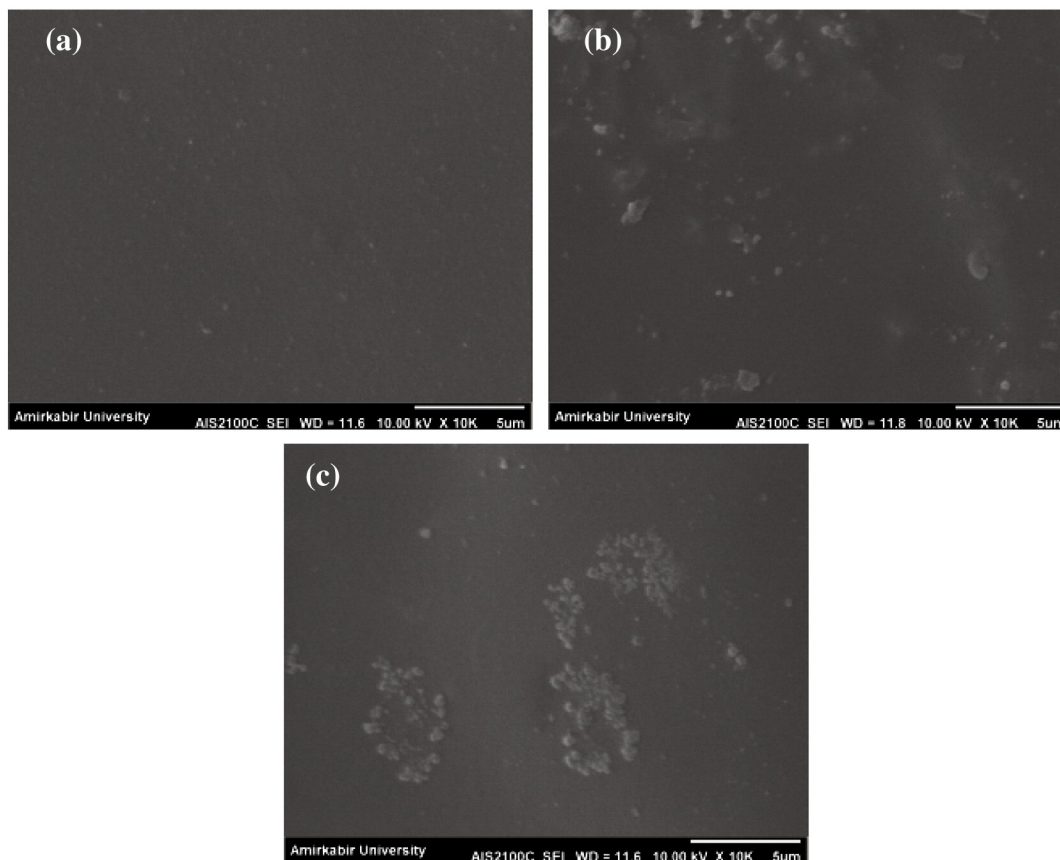

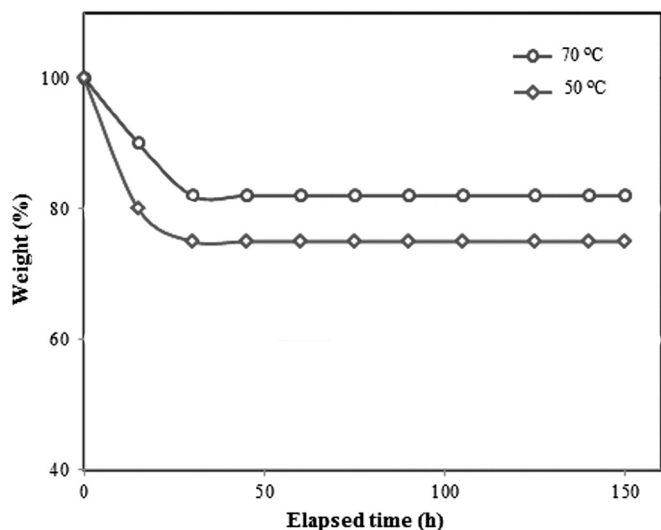**Fig. 5.** SEM images of the cross-section of (a) PPB$_1$, (b) PPB$_{1.2}$ and (c) PPB$_{1.5}$ nanocomposite membranes.

Fig. 6. Time course of weight loss of PPB$_1$ nanocomposite membranes in Fenton's reagent at 50 °C and 70 °C.

BaZrO$_3$ is a rebellious ceramic material which is actually promising due to its high melting point (2920 °C) and low chemical reactivity with corrosive compounds. Unlike most of the perovskite systems, BaZrO$_3$ does not undergo any (long-range-order) structural phase transition and thus remains cubic and paraelectric down to 2 K.

In addition, BaZrO$_3$ has excellent thermal stability and resistance due to low coefficient of thermal expansion ($\alpha = 87 \times 10^{-7}/°C$ between 25 °C and 1080 °C) [21,22].

GA as cross linking agent causes PVA structure to become more compacted and rigid, resulting in a decrease in the free volume capable of containing water molecules [47] and an increase in the thermal stability of nanocomposite membranes compared with PVA based membrane. PVP and BaZrO$_3$ nanoparticles are strongly hydrophilic components and in appropriate amount can produce membranes with good thermal and water uptake properties. It is of note that the PEMFCs are used mostly below 250 °C, and all the prepared membranes in this study have good thermal stability in this range. However, TGA plots at temperatures above 250 °C show that the thermal stability of the PB and PPB membranes is improved due to the BaZrO$_3$ nanoparticles. PPB nanocomposite membranes due to high polarity of $-N-C=O$ group of PVP, which makes strong hydrogen-bonding with PVA and intense intra-molecular interaction [24], displayed a higher thermal stability than PB nanocomposite membranes. The high thermal stability of PPB$_1$ nanocomposite membranes, confirmed their capabilities at high temperature PEMFCs.

due to hydrogen bonding and –OH single vibration [45]. The high intensity of the –OH peak in the PPB nanocomposite membranes compared with PVA membranes, because of hydrogen bonding of PVP, was also clearly observed. The bands at 2907 cm^{-1} and 1324–1422 cm^{-1} were attributed to the C–H stretching and bending vibrations of methylene groups respectively [12]. The peak around 2850 cm^{-1} suggests the presence of such free aldehyde groups [46]. The peak at 1720–1730 cm^{-1} suggests the presence of such free C=O groups, but was apparently covered by vicinity band in this region [46,47]. The presence of PVP in the PPB nanocomposite membrane was confirmed by the bands assigned to the C=O and N–C stretching vibrations at 1657–1674 cm^{-1} [48]. The peak at 1000 cm^{-1} was assigned to the C–O groups of PVA based membrane. The presence of –OH groups in the PVA chain allows the reaction with –CHO groups in GA and formation of ether bonds (C–O–C). The bands at 1200–1250 cm^{-1} were attributed to the C–O–C bonds [45].

3.5. Mechanical properties

From Table 1 it was found that the nanocomposite membranes due to strong interactions of BaZrO$_3$ nanoparticles with PVA based membrane, displayed a higher mechanical stability than PVA based membrane. BaZrO$_3$ nanoparticles have excellent mechanical stability [20] and an increase in mechanical stability of PVA based nanocomposite membranes when incorporated in PVA matrix The PPB$_1$ nanocomposite membranes because of the strong interfacial interactions of PVP show the best mechanical properties. Dispersion of the Ba and Zr nanoparticles in the cross-section of PPB$_1$ nanocomposite membrane was investigated by the EDX mapping images and displayed in Fig. 9. EDX distribution demonstrated homogenous distribution of Ba and Zr nanoparticles in the PPB nanocomposite membranes.

Uniform dispersion of nanoparticles in the PPB$_1$ nanocomposite membranes, which increases the PVA-nanoparticle interactions, also plays a key role in the improvement of its mechanical stability. PPB$_1$ nanocomposite membranes are adequate to be fabricated into membrane electrode assemblies.

3.4. Thermal properties

From Fig. 8, PB$_1$ and PPB$_1$ nanocomposite membranes demonstrated a higher thermal stability than PVA based membrane. Incorporation of BaZrO$_3$ nanoparticles in PVA polymer matrix leads to the increase of decomposition temperature of nanocomposite membranes compared with PVA based membrane. Among the perovskites with cubic structures,
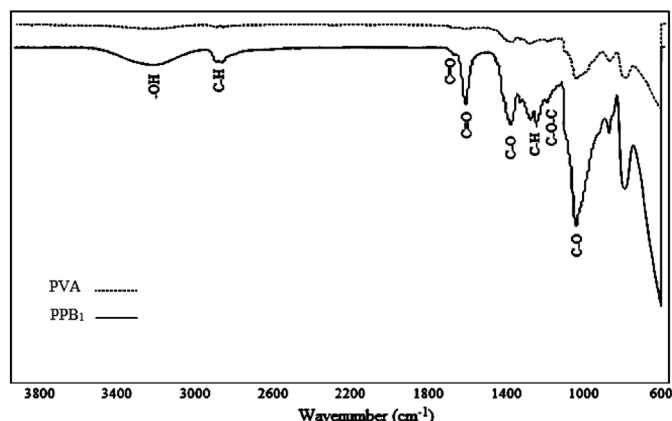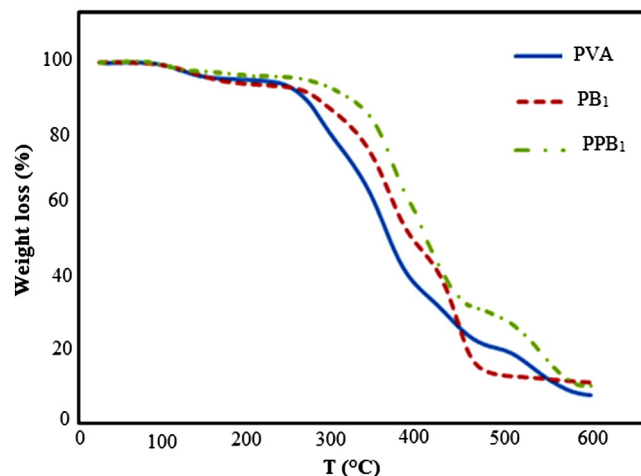

Fig. 7. FT-IR ATR spectra of PVA and PPB$_1$ membranes.

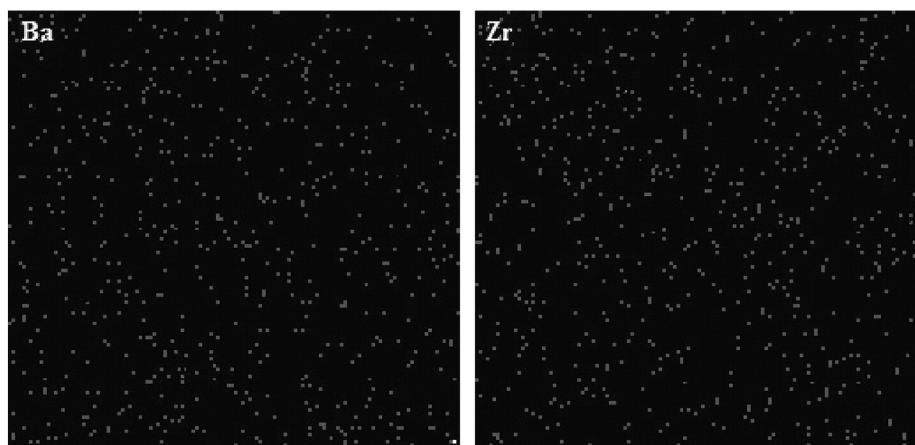Fig. 8. TGA plots of PVA, PB$_1$ and PPB$_1$ membranes.

Fig. 9. EDX distribution of Ba and Zr nanoparticles in the cross-section of PPB$_1$ nanocomposite membranes.

3.6. Fuel cell performance

The PPB$_1$ nanocomposite membranes were also used for their performance assessment in H$_2$/O$_2$ PEMFCs by making membrane electrode assemblies (MEAs). The catalyst loading on both the anode and the cathode (active area = 5 cm^2) was kept at 0.5 mg/cm^2.

Fig. 10 depicts i-V and power density curves for the PEMFCs using PPB$_1$ nanocomposite membranes at 25, 50 and 70 °C. Clearly, an increase in the fuel cell temperature leads to a dramatic enhancement in the cell performance. Temperature is an important parameter that improves electrochemical properties of fuel cells. The maximum power density of 9.47 mW/cm^2 is observed at 0.16 V with a peak current density of 58 mA/cm^2 for PPB$_1$ nanocomposite membranes at 25 °C, as listed in Table 4. This peak is shifted to higher current (201 mA/cm^2) with a higher power density (29 mW/cm^2) with increasing temperature of up to 70 °C. This result was comparatively higher than other reported results [7,32,41,49]. The PPB$_1$ nanocomposite membrane exhibited a high power performance at 29 mW/cm^2 at 70 °C, and a similar performance at 80 °C (22 mW/cm^2) [50].

The open-circuit voltage (OCV) is determined when there are no current flows into the fuel cell. This is known as the initial voltage
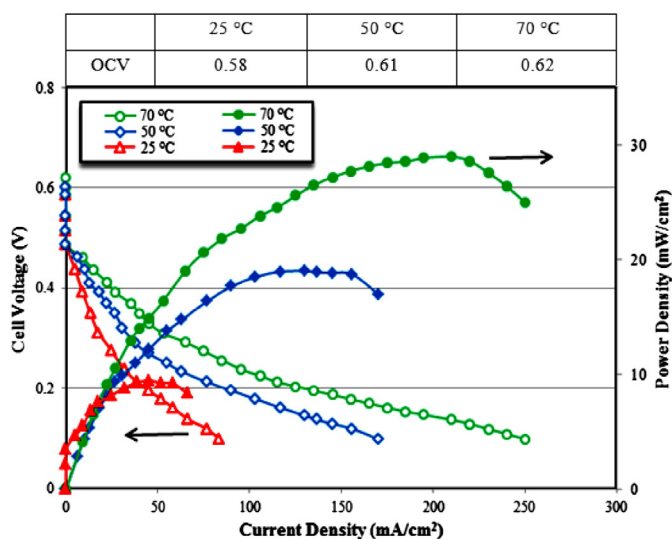
prior to the cell voltage measurement. The open circuit voltage detected for PPB$_1$ nanocomposite membranes in 70 °C was about 0.62 V.

The polarization curve can be separated into three different regions: activation overvoltage (initial fall in voltage), ohmic overvoltage and concentration overvoltage. Activation overvoltage corresponds to the energy barrier that must be overcome to initiate a chemical reaction between reactants. Activation overvoltage is a major source of voltage loss when the current density is small. In low- and medium-temperature fuel cells, activation overvoltage is the most important irreversibility and cause of voltage drop. At higher temperatures and pressures the activation overvoltage becomes less important. Ohmic overvoltage occurs due to resistive losses in the cell. Concentration overvoltage is the voltage loss due to reactant starvation.

In fact, similar initial drops in voltage were found with different membranes, electrodes and MEA fabrication procedures when using the same instrumental apparatus (a loss of 150–200 mV was constantly detected directly after applying a load) [43].

The increase in power density of PPB$_1$ nanocomposite membranes as it increases the temperature is powerful due to the higher proton conductivity. Several protons with higher mobility are permitted to be transported from anode to cathode if the membrane is conductive. Consequently, higher proton conductive specific of PPB$_1$ nanocomposite membranes promotes the exchange of the fuel into electricity through a redox process in a fuel cell system and so increases the power density of the fuel cell.

It is of note that although the power density of the PPB$_1$ nanocomposite membrane based MEA (29 mW/cm^2 at 0.14 V) is lower than the commercial Nafion 117 based MEA (500 mW/cm^2 at 0.5 V), the PPB nanocomposite membranes can be made with very simple and potentially very cheap technology.

3.7. MEA life test

The result of an 87 h life test of PPB$_1$ nanocomposite membrane unit cell operated at 70 °C under a constant current loading (i = 25 mA/cm^2) is shown in Fig. 11. During each 24-hour the life test was interrupted (12 times), including four complete shut downs. 60 h after the test started

Fig. 10. Comparison of i-V and power density curves for the PEMFCs using PPB$_1$ nanocomposite membranes. The cell temperature is at 25 °C, 50 °C and 70 °C with 1 atm pressure. The anode and cathode Pt loadings were both 0.5 mg/cm^2. Each MEA with an active area of 2.3 × 2.3 cm^2 was performed with the fuel cell test with the H$_2$/O$_2$ flow rates at 300/500 ml/min.

Table 4
Electrochemical parameters for the PEMFCs using the PPB$_1$ nanocomposite membrane.

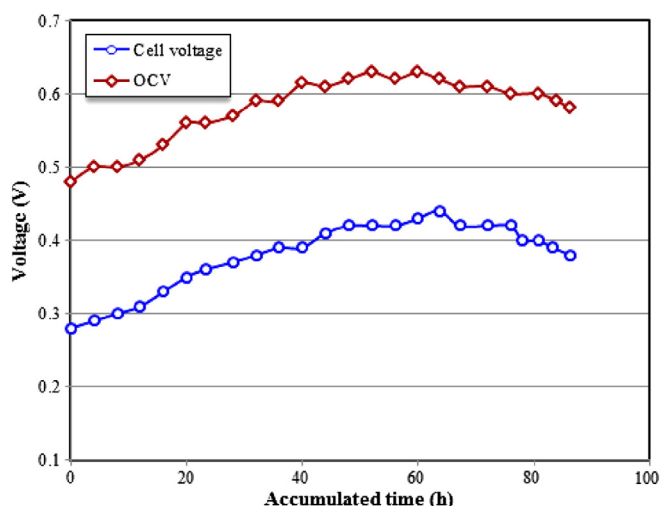| Parameters	T (°C)		
	25 °C	50 °C	70 °C
E_{ocv}/V	0.58	0.61	0.62
Max.P.D./(mW/cm^2)	9.5	19	29
$i_{p,max}$/(mA/cm^2)	58	130	210
$E_{p,max}$/V	0.16	0.15	0.14

Fig. 11. PPB$_1$ nanocomposite membrane based MEA unit cell life test under a constant current loading (i = 25 mA/cm^2) and an ambient pressure. The cell temperature was 70 °C and the anode and cathode Pt loadings were both 0.5 mg/cm^2.

the cell voltage reached maximum value (0.62 V) and then gradually decreased. However, by the end of the life test the cell voltage was even higher than the cell voltage recorded at the opening of the test. During the beginning of the 60 h test, the cell voltage increased from 0.48 V to 0.62 V. A slight decline of voltage from 0.62 V to 0.58 V was detected from 60 h to 87 h. Under a fixed loading current for a long time fuel cell test, two regions were observed in the output voltage versus testing time curve. The first initial testing period was the "activation region" in which cell voltage increased with operating time. The improvement of fuel cell performance at the "activation region" is due to the better contact of membrane with catalyst layers by the pressure of the end plates and expansion of the interface for the electrochemical reaction [51]. Following the "activation region" was the "decline region", in which the cell voltage decreased with operating time. The decline of cell voltage during the latter stage of life test was due to the loss of PVP from the membrane. Loss of PVP from nanocomposite membrane structure decreases the proton conductivity and fuel cell performance.

4. Conclusion

Advanced nanocomposite membranes based on PVA/PVP/BaZrO$_3$ were prepared by solution casting method. PVA, PVP and BaZrO$_3$ were used as based polymer, blend polymer with PVA and inorganic modifier, respectively. Glutaraldehyde (GA) was used as crosslinking agent. The nanocomposite membranes with 1 wt.% of BaZrO$_3$ nanoparticle in the presence of PVP due to the strongly hydrophilic character of PVP and BaZrO$_3$ nanoparticles, showed a higher water uptake and proton conductivity compared to those of the PVA based membrane. PVA/PVP/BaZrO$_3$ nanocomposite membranes (with 1 wt.% of nanoparticle) displayed 6×10^{-2} S/cm at 70 °C. The strong surface interactions of BaZrO$_3$ nanoparticles and great interfacial interactions of PVP increase the mechanical properties of nanocomposite membranes. The results of SEM-EDX analysis have provided detailed information about the homogenous distribution of nanoparticles in the nanocomposite membranes. The electrochemical performance, in terms of the maximum power density, of the PEMFC for PVA/PVP/BaZrO$_3$ nanocomposite membranes (1 wt.% of BaZrO$_3$ nanoparticle) was found at 29 mW/cm^2 at 70 °C. Proton conductivity measurements and fuel cell tests approved the best properties of PVA/PVP/BaZrO$_3$ nanocomposite membranes among the numerous compositions explored and established the potentiality of the prepared nanocomposite membranes as electrolytes in fuel cell devices.

References

[1] J.M. Andujar, F. Segura, Renew. Sustain. Energy Rev. 13 (2009) 2309–2322.
[2] A.J. Appleby, F.R. Foulkes, Fuel Cell Handbook, Van Nostrand Reinhold, New York, 1989.
[3] C.Y. Chen, J.I. Garnica, M.C. Duke, R.F. Dalla, A.L. Dicks, J.C. Diniz, J. Power Sources 166 (2007) 324–330.
[4] Z. Wu, G. Sun, W. Jin, H. Hou, S. Wang, Q. Xin, J. Membr. Sci. 313 (2008) 336–343.
[5] R.K. Nagarale, W. Shin, P.K. Singh, J. Polym. Chem. 1 (2010) 388–408.
[6] A. Martinelli, M.A. Navarra, A. Matic, S. Panero, P. Jacobsson, L. Börjesson, Electrochim. Acta 50 (2005) 3992–3997.
[7] C.C. Yang, W.C. Chien, T.J. Li, J. Power Sources 195 (2010) 3407–3415.
[8] D.S. Kim, H.B. Park, J. Rhim, Y.M. Lee, J. Membr. Sci. 240 (2004) 37–48.
[9] C.E. Tsai, C.W. Lin, J. Rick, B.J. Hwang, J. Power Sources 196 (2011) 5470–5477.
[10] D.S. Kim, H.I.I. Cho, D.H. Kim, B.S. Lee, S.W. Yoon, Y.S. Kim, G.Y. Moon, H. Byun, J. Rhim, J. Membr. Sci. 342 (2009) 138–144.
[11] J.W. Rhim, H.B. Park, C.S. Lee, J.H. Jun, D.S. Kim, Y.M. Lee, J. Membr. Sci. 238 (2004) 143–151.
[12] H. Beydaghi, M. Javanbakht, H. Salar Amoli, A. Badiei, Y. Khaniani, M. Ganjali, P. Norouzi, M. Abdouss, Int. J. Hydrogen Energy 36 (2011) 13310–13316.
[13] H. Beydaghi, M. Javanbakht, A. Badiei, J. Nanostruct. Chem. 97 (2014), http://dx.doi.org/10.1007/s40097-014-0097-y.
[14] P. Salarizadeh, M. Javanbakht, M. Abdollahi, L. Naji, Int. J. Hydrogen Energy 38 (2013) 5473–5479.
[15] P. Salarizadeh, M. Abdollahi, M. Javanbakht, Iran. Polym. J. 21 (2012) 661–668.
[16] Kh. Hooshyari, M. Javanbakht, L. Naji, M. Enhessari, J. Membr. Sci. 454 (2014) 74–81.
[17] E. Caetano Camilo de Souza, R. Muccillo, J. Mater. Res. 13 (2010) 385–394.
[18] Kh. Hooshyari, M. Javanbakht, A. Shabanikia, M. Enhessrar, J. Power Sources (2014), http://dx.doi.org/10.1016/j.powsour.2014.11.083 (in press).
[19] M. Cherry, M.S. Islam, J.D. Gale, C.R.A. Catlow, J. Phys. Chem. 99 (1995) 14614–14618.
[20] A. Azad, S. Subramaniam, T. Wan Dung, J. Alloys Compd. 334 (2002) 118–130.
[21] S. Parida, S.K. Rout, L.S. Cavalcante, E. Sinha, M. Siu Lic, V. Subramanian, N. Guptae, V.R. Gupta, J.A. Varela, E. Longo, Ceram. Int. 38 (2012) 2129–2138.
[22] L. Ciontea, T. Ristoiu, R. Suciu, T. Petrisor, B. Neamtu, A. Rufoloni, G. Celentano, T. Petrisor, J. Optoelectron. Adv. Mater. 9 (2007) 776–779.
[23] M. Enhessari, S. Khanahmadzadeh, K. Ozaee, J. Iran. Chem. Res. 3 (2010) 11–15.
[24] J. Qiao, T. Hamaya, T. Okada, Polymer 46 (2005) 10809–10816.
[25] Q. Zhang, G. Wahnstrom, M. Bjorketun, S. Gao, E. Wang, Phys. Rev. Lett. 101 (2008) 215902.
[26] S. Stokes, M. Saiful Islam, J. Mater. Chem. 20 (2010) 6258–6264.
[27] T. Onishi, T. Helgaker, A Theoretical Study on Proton Conduction Mechanism in BaZrO$_3$ PerovskiteChapter 14 Springer International Publishing, Switzerland, 2013.
[28] W. Zajac, D. Rusinek, K. Zheng, J. Molenda, Cent. Eur. J. Chem. 11 (2013) 471–484.
[29] M. Cherry, M. Islam, J. Gale, C. Catlow, J. Phys. Chem. 99 (1995) 14614–14618.
[30] W. Munch, G. Seifert, K. Kruer, J. Maier, Solid State Ionics 97 (1997) 39–44.
[31] M. Cherry, M. Islam, J. Gale, C. Catlow, Solid State Ionics 77 (1995) 207–209.
[32] Y. Chun-Chen, J. Shingjiang, S. Jeng-Ywan, J. Power Sources 196 (2011) 4458–4467.
[33] N.V. Dale, M.D. Mann, H. Salehfar, A.M. Dhirde, T. Han, J. Fuel Cell Sci. Technol. 7 (2010) 1–10.
[34] X. Yuan, H. Wang, J.C. Sun, J. Zhang, Int. J. Hydrogen Energy 32 (2007) 4365–4380.
[35] M. Hem, S. Selvas, H. Nithy, A. Sakuntha, Ionics 15 (2009) 487–491.
[36] D.S. Kim, M.D. Guiver, S. Nam, T.I. Yun, M. Seo, S.J. Kim, et al., J. Membr. Sci. 281 (2006) 156–162.
[37] L. Li, Xu, Y. Wang, Mater. Lett. 57 (2003) 1406–1410.
[38] B.P. Tripathi, A. Saxena, V.K. Shahi, J. Membr. Sci. 318 (2008) 288–297.
[39] Y. Jin, J. Costa, G. Lu, Solid State Ionics 178 (2007) 937–942.
[40] A. Anis, A.K. Banthia, S. Bandyopadhyay, J. Power Sources 179 (2008) 69–80.
[41] M.A. Navarra, A. Fernicola, S. Panero, A. Martinelli, A. Matic, J. Appl. Electrochem. 38 (2008) 931–938.
[42] U. Thanganathan, J. Parrondo, B. Rambabu, J. Appl. Electrochem. 41 (2011) 617–622.
[43] D. Kim, M. Guiver, M. Seo, H. Cho, D. Kim, J. Rhim, G. Moon, S. Nam, Macromol. Res. 15 (2007) 412–417.
[44] S. Shanmugam, B. Viswanathan, T. Varadarajan, J. Membr. Sci. 275 (2006) 105–109.
[45] M.S. Kang, Y.J. Choi, S.H. Moon, J. Membr. Sci. 207 (2002) 157–170.
[46] H.S. Mansur, C.M. Sadahira, A.N. Souza, A.A.P. Mansur, Mater. Sci. Eng. C 28 (2008) 539–548.
[47] Y. Wu, C. Wu, Y.X.T. Li, Y. Fu, J. Membr. Sci. 350 (2010) 322–332.
[48] B. Yuri, E.H. Susan, K. Matthias, Y. Peidong, F. Heinz, A.S. Gabor, J. Phys. Chem. B 110 (2006) 23052–23059.
[49] T. Yang, J. Membr. Sci. 342 (2009) 221–226.
[50] J. Qiao, T. Okada, J. New Mater. Electrochem. Syst. 10 (2007) 231–236.
[51] H. Lin, Y. Hsieh, C. Chiu, T. Yu, L. Chen, J. Power Sources 193 (2009) 170–174.